Overall Efficiency of Ducted Tidal Current Turbines

M. Shives[1] and C. Crawford[2]
Dept. of Mechanical Engineering, University of Victoria
PO Box 3055
Victoria, B.C. Canada V8W 3P6

[1]E-mail: mrshives@uvic.ca
[2]E-mail: curranc@uvic.ca

***Abstract*-Computational fluid dynamics (CFD) simulations have been completed to characterize the efficiency of tidal turbines. Efficiency is taken as the ratio of power production (i.e. useful electricity) to total power lost from the upstream incident flow energy. Many tidal turbine developers are considering ducted designs which accelerate the flow through the turbine, improving the power coefficient C_P. It has been found that for the designs considered, this increase in C_P is associated with decreasing efficiency due to increased overall drag of the entire system. It is also found that for a given turbine, the optimum operating condition for power differs from the optimum condition for efficiency. Thus a compromise between power and efficiency must be made when considering turbines in constricted waters and arrays of turbines.**

I. Introduction

Marine current turbines are showing increasing suitability as a sustainable energy technology in areas where significant tidal flows occur. North America has a significant tidal resource which has only been partially assessed. Potential sites that have been studied in some detail include the Johnstone Strait [1], the Bay of Fundy [2], and Puget Sound [3]. Several concepts have emerged for tidal current turbine designs, many of which incorporate a duct which increases the mass flow through the turbine, thus enhancing its power. Such designs allow a given power output to be achieved with a smaller diameter turbine operating at a faster rotational speed. These features are expected to give ducted turbines an economic advantage over their open flow counterparts.

It is important to understand that there is a limit to the amount of energy that can be extracted from tidal flows. Garrett and Cummins [4] have developed a model to assess the limits to tidal power extraction in a channel. Their model computes the total energy available, which is finite and should therefore be harnessed with a minimum of losses. Adding turbines to a channel will impose drag forces which reduce the flow velocity and therefore reduce its energy content. A component of the drag arises inherently due to power production, while drag due to supporting structures and ducts does not contribute to power generation and effectively reduces the total available flow energy. If an array of many turbines is to be installed, the reduction of total energy available will be significant.

In comparing ducted and open-flow turbines there are essentially two competing factors; one is the power augmentation due to increased mass flow and the other is the increased drag. The research presented in this paper characterizes the efficiency of marine current turbines in terms of the ratio between the power produced by the rotor (neglecting any mechanical or electrical losses) and the total power lost from the flow (the sum of power production and drag losses). This allows the relative magnitude of the power augmentation and increased drag to be expressed with a single parameter providing a basis for comparing various ducted and open flow designs in terms of their overall energy extraction. Relative to wind turbine performance metrics, this efficiency evaluation is important given the relative restrictions on tidal flows compared to unconstrained wind fields.

II. Methodology

A. Actuator Disk Approach

Several ducted turbine designs have been simulated using computational fluid dynamics (CFD) software. The simulations use an actuator disk approach where the turbine is represented by a momentum sink region within the flow domain. This allows the effect of the turbine to be modeled without the need to resolve the blades explicitly, greatly reducing the number of nodes required. This approach also allows more nodes to be allocated to resolving the boundary layer flow of the duct as well as the shear layer at the edge of the wake. This approach also serves as an upper bounding case for real rotor performance. The duct and actuator disk are depicted in Fig. 1, which also shows the stations where flow parameters are evaluated: 0) free-stream, 1) duct entrance, 2) actuator disk entrance, 3) actuator disk exit, 4) duct exit, 5) far wake, and 6) very far wake. The subscripts used in this paper correspond to these station numbers.

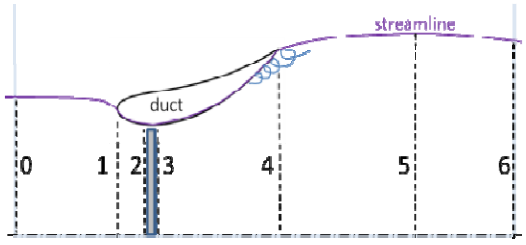

Figure 1: Stations diagram

Funding provided by: Natural Sciences and Engineering Research Council of Canada (NSERC), Pacific Institute for Climate Studies (PICS) and the University of Victoria

B. Defining Efficiency

In this paper the efficiency is defined as the power produced by the turbine divided by the total power lost from the flow (3). Using the actuator disk approach [5], the turbine power P is simply the product of the local flow velocity u_0 and the turbine thrust T (1). The power lost from the flow, which is equivalent to the total work done on the flow by all parts of the turbine system, is simply the sum of the turbine thrust and drag D (from the duct, structures, and the turbine blades themselves) multiplied by the freestream velocity (2). This simple definition of loss has been noted by Corten [6], and can be deduced by considering a system where the turbine with all its structures is pulled through a stationary fluid at a velocity u_0. The power required to pull the turbine is simply the force applied multiplied by the velocity, and is equal to the power lost from the flow in the case of a stationary turbine in a moving fluid. In fact of course the energy lost from the flow not owing to the useful power extraction in the rotor ends up as thermal energy after viscous dissipation completes, however the heat capacity of the flow is so large that the results are unaffected by considering this temperature change.

$$P = Tu_2 \tag{1}$$

$$P_E = (T + D)u_0 \tag{2}$$

$$\eta = \frac{P}{P_E} = \frac{T}{(T + D)}\frac{u_2}{u_0} \tag{3}$$

By defining a velocity ratio $\alpha = u_2/u_0$ and a drag factor $\beta = D/T$, the efficiency can be expressed simply as in (4). Note that the velocity ratio α is related to the more commonly used axial induction factor a by $\alpha = (1 - a)$. The power and thrust terms are often normalized by the freestream velocity u_0, fluid density ρ, and rotor swept area A_R. In this study the duct drag is normalized in the same manner. The normalized parameters C_T, C_D, C_P and C_{PE} are defined in equations (5) to (8).

$$\eta = \frac{\alpha}{1 + \beta} \tag{4}$$

$$C_T = \frac{2T}{\rho u_0^2 A_R} \tag{5}$$

$$C_D = \frac{2D}{\rho u_0^2 A_R} \tag{6}$$

$$C_P = \frac{2P}{\rho u_0^3 A_R} = \alpha C_T \tag{7}$$

$$C_{PE} = \frac{2P_E}{\rho u_0^3 A_R} = C_T + C_D = C_T(1 + \beta) \tag{8}$$

The present research compares the efficiency of ducted turbines to their open flow counterparts. At this preliminary stage, ideal turbines are assumed such that there is no drag due to supporting structures or due to the turbine blades. Only the drag due to the duct is considered in determining the efficiency of each ducted design.

C. The Open Flow Case

In the open flow case, the turbine efficiency can be calculated based on standard 1D actuator disk theory [5]. The local velocity u_2 is assumed uniform over the actuator disk and is defined as $u_2 = u_0(1 - a)$ where a is the axial induction factor. By momentum theory, the induction factor is related to the thrust coefficient $C_T = 2T/(\rho u_0^2 A_2)$ according to (9). At high thrust coefficients (above approximately $8/9$) the momentum theory breaks down due to the turbine entering the turbulent wake state where momentum from the exterior flow is entrained into the wake. In this state, the induction factor is calculated by an empirical formula which fits a straight line from the value of C_T at the transition to turbulent wake state to a value C_{T1} when the induction factor $a = 1$. In this paper C_{T1} is taken as 1.7 and (10) is used to find the induction factor in the turbulent wake state. The efficiency of the ideal open flow turbine is then calculated from (3) with $D = 0$ and $u_2 = u_0(1 - a)$, which simplifies to (11).

$$a = \tfrac{1}{2}\left(1 - \sqrt{1 - C_T}\right) \tag{9}$$

$$a = 1 - \frac{C_{T1} - C_T}{4\left(\sqrt{C_{T1}} - 1\right)} \tag{10}$$

$$\eta = (1 - a) \tag{11}$$

D. The Ducted Case

In the ducted case, the efficiency is calculated based on simulation results where the velocity u_2 varies radially. In the simulation, the actuator disk is a subdomain in which a uniform force per unit volume fx is applied to the flow within each control volume. Thus the turbine thrust T is the volume integral of fx over the disk volume. The duct drag D is the area integral of the local force in the x direction (with pressure and shear components) over the duct surface. The turbine power P is the volume integral of the product of fx and the local axial velocity u, which varies radially and across small but finite thickness of the disk (the disk thickness is less than 5% of its radius). The total extracted power P_E is the product of (T+D) and U_0. The efficiency is simply calculated as the ratio of P and P_E.

III. Duct Geometry

To avoid making generalizations based on a single design, several duct geometries were tested. The geometric parameters expected to impact the duct performance were the diffuser expansion ratio A_4/A_3; the inlet contraction ratio A_1/A_3; the duct profile thickness ratio; and the inner and outer diffuser surface angles $\theta_{4,in}$, $\theta_{4,out}$ as depicted in Fig 1.

Duct geometries were created following a similar methodology to Hansen [7] in his CFD simulation. A baseline geometry (case 2) was designed to replicate Hansen's duct for model comparison. The duct profile was based on a NACA 0015 airfoil which was first scaled in thickness by a factor k_t. A camber was then applied by rotating the geometry through a linearly varying angle (0 at the leading edge to θ_1 at the trailing edge). A full body rotation through θ_2 was then applied to the entire cross section. Finally the airfoil was

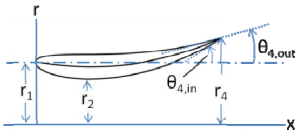

Figure 2: Geometric Attributes

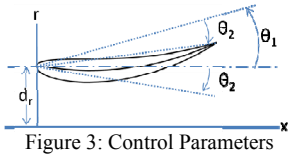

Figure 3: Control Parameters

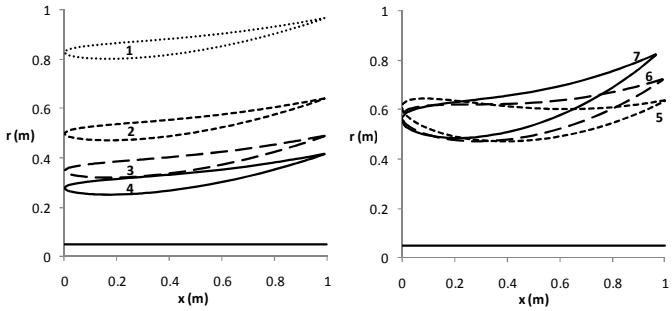

Figure 4: Duct profiles for cases 1-4 (left) and cases 5-7 (right)

translated by *dr* to control the throat area A_2. These control parameters are depicted in Fig 2. This methodology allows full control over a wide variety of duct area ratios and angles. The above control parameters and resulting duct area ratios and outlet angles are summarized in Table 1 for the seven ducts used in this study.

Cases 1 through 4 differed only in the *dr* term and have the same exit angles and thickness ratios. This allows effects due to changing the area ratios to be isolated. Cases 5 through 7 were designed such that the diffuser outlet angles increase as the diffuser expansion ratio increases. The diffuser expansion ratios for cases 5-7 were set to correspond to those for cases 2-4; allowing effects due to the outlet angles to be observed.

IV. CFD Simulation

A. General Description

CFD simulations were carried out using ANSYS CFX, following a similar methodology to that of Hansen [7]. The simulations use an axi-symmetric actuator disk model without swirl to produce results that are readily used to calculate the efficiency. The mesh is a 15° slice of the entire flow domain. Periodic boundary conditions were enforced to simulate the entire 360° domain. This mesh was realized by sweeping a 2D structured surface mesh through a 15° rotation using five elements. The mesh was refined in proximity to the duct surface and actuator disk. The turbulence was modeled using the k-ω SST option due to its good performance in predicting boundary layer separation with adverse pressure gradients. No model for the transition from laminar to turbulent flow was used as the flow is expected to be turbulent along the entire duct surface.

Distances were normalized based on the duct length L=1 m. The simulation domain inlet was 5L upstream of the duct leading edge and employed a uniform velocity. The outlet was 10L downstream of the trailing edge and enforces $p=p_0$. As in Hansen [7] an inner radial boundary employing a free-slip condition was located at 0.05L to avoid a singularity in azimuthal velocity at the centerline. The outer radial boundary was located at r=5L and was treated using the opening for entrainment option, which approximates an infinite domain. The sensitivity of the simulated C_P to moving the outer radial boundary to 10L was less than 1%; this was considered acceptable.

The actuator disk was simulated as a momentum sink where a force per unit volume f_x was applied at each element. The disk was located at the duct throat. The force distribution was uniform over the actuator disk. The f_x term was calculated based on the actuator disk thickness and the desired thrust coefficient for each simulation. To be consistent with the simulation by Hansen, a small gap of width $0.08r$ was left between the outer radius of the actuator disk and the surface of the duct. As shown by Hansen, this gap accelerates the boundary layer flow and is thought to delay flow separation. This effect would not be present in a real turbine with a discrete number of blades unless the solidity ratio was very high. The gap was used nonetheless to maintain consistency with Hansen for subsequent validation.

The actuator disk CFD methodology has been validated for the non-ducted rotor case and was found to reproduce the standard actuator disk theory well as shown in Fig. 5. (Note that the empirical thrust correction (10) was applied for $C_T > 8/9$ to account for momentum theory breakdown at high thrust).

B. Grid Refinement Study

To ensure minimal grid resolution error, the effect of grid refinement on the power coefficient and rotor plane induction was studied using the baseline duct geometry. Adequate resolution of the boundary layer along the duct was considered crucial. It was found that the simulated power coefficient varied nearly linearly with the 1st layer spacing in the boundary layer region. A sample plot is shown in Fig. 6 for C_T 0.9. The linear trend was used to determine the expected C_P with an infinitesimally small spacing. This allowed a calculation of the expected resolution error for each mesh. The final mesh had a 1st layer spacing of 0.08 mm and the expected error in C_P was less than 1% for C_T ranging from zero to one. This mesh spacing gave a y^+ value less than 10 at all points along the duct.

TABLE I
CONTROL PARAMETERS AND RESULTING ATTRIBUTES

CASE	Control Parameters				Duct Attributes			
	k_t	θ_1	θ_2	d_y	A_4/A_2	A_1/A_2	$\theta_{4,L}$	$\theta_{4,U}$
1	0.45	8.08	0.00	0.83	1.47	1.07	19.95	11.37
2	0.45	8.08	0.00	0.50	1.84	1.12	19.95	11.37
3	0.45	8.08	0.00	0.35	2.36	1.18	19.95	11.37
4	0.45	8.08	0.00	0.28	2.87	1.24	19.95	11.37
5	1.00	20.00	-18.92	0.62	1.84	1.73	27.57	10.27
6	1.00	20.00	-11.65	0.58	2.36	1.50	34.84	17.54
7	1.00	20.00	-5.00	0.56	2.87	1.34	41.49	24.19

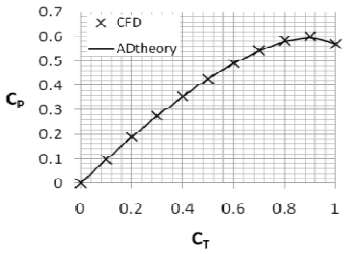

Figure 5: Comparison of CFD method to actuator disk theory

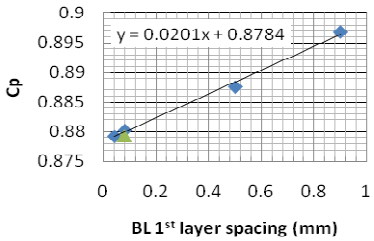

Figure 6: Effect of boundary layer mesh size on CP

The same strategy was used to study the axial spacing, which was refined at the duct inlet, outlet, and at the rotor plane. It was found that with a minimum axial spacing of 0.5 mm at the trailing edge, the expected C_P error was less than 1% over the full range of C_T. The final mesh consisted of 467 elements in the axial direction, 43 elements crossing the boundary layer refinement O-grid, and 142 elements in the radial direction. The total number of elements was 313 530.

C. CFD Comparison to Hansen

The baseline duct geometry was a replica of that simulated by Hansen. As a validation of the CFD model, the C_P-C_T relationship was compared to Hansen's result as shown in Fig. 6. The maximum C_P in the present simulations is 3% lower than Hansen's result. This discrepancy is likely due to minor differences in duct geometry and meshing strategy, but is considered acceptable.

V. RESULTS

Using the methodology presented in section II the open flow turbine efficiency and power coefficient were calculated as a function of C_T. Using the simulation results, the ducted turbine efficiency and power coefficient have been calculated for each design. The results are plotted in Fig. 8. It can be seen that the ducted designs show a significant improvement in power coefficient over the open turbine, but at a cost of reduced efficiency. Based on the results obtained to date, it appears

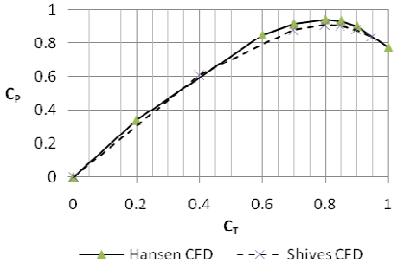

Figure 7: Comparison to Hansen's result.

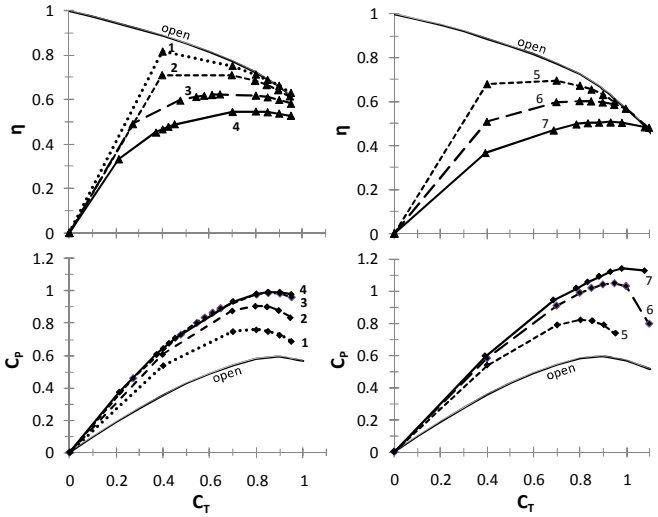

Figure 8: Efficiency and power coefficient for ducted and open designs

that the efficiency of all ducted turbines is bounded by the ideal open turbine case. This seems reasonable since the ideal open case assumes zero losses due to drag, and therefore represents a maximum possible efficiency.

The general trend for cases 1 through 4 is an increase in maximum C_P as the diffuser expansion ratio A_4/A_3 increases up to approximately 2.4 (case 3); beyond this expansion ratio no further improvement is noted. For cases 5 to 7, C_P inc ased as the duct outlet angl (along with the expansion ratio) increased. In general, as the duct had more influence on the flow (whether through increasing expansion ratio, or increasing outlet angle) the overall efficiency became lower. This is physically reasonable. If the power enhancement is thought of as being caused by increased circulation due to the duct lift force [7] then it is clear that as the lift increases the induced drag will increase as well, degrading the overall efficiency. Note that the duct with the best performance enhancement (case 7) also showed the greatest reduction in efficiency.

The power improvement by the duct is sometimes attributed to a base pressure effect [8,9,10] which arises when recirculation behind the duct provides a low pressure region which acts to accelerate the flow through the duct. This effect is closely linked to the circulation concept mentioned above, but is associated with the duct airfoil section approaching and entering the stalled condition. In stall, flow separation is evident in the interior flow, leading to the base pressure effect. The problem with stalled flow is the sharp rise in drag as stall occurs. While exploiting the base pressure effect improves the power coefficient of a ducted turbine, this strategy drastically reduces the overall system efficiency. The second problem with stalled flow is that the recirculation region aft of the airfoil limits the final expansion of the wake, which in turn limits the C_P enhancement. So on one hand it accelerates the flow by providing a low pressure region aft of the turbine, but on the other it limits wake expansion.

Fig. 9 shows the region of reversed flow (shown in black) behind the ducts 5 and 7. It is clear that the case 7 duct is in a stalled condition and has a correspondingly high drag coefficient as shown in Fig. 10. The case 5 duct is the same airfoil but is oriented at an angle of attack smaller than the critical angle where stall sets in. It has a very small region of reversed flow and a small drag coefficient (Fig. 10).

VI. Effect of Structural Drag

The analysis described above would seem to imply that the open turbine is inherently more efficient than the ducted type. However this is not necessarily the case as the preceding analysis neglected many inefficiencies for both design types. A more thorough study is underway to quantify losses due to structural drag, tip loss, and blade drag. Swirl and free-surface effects are also being included to ascertain their effects on the results.

An approximate estimate of the structural drag for a typical open turbine can be made based on the SeaGen turbine [11]. The design features two rotors connected side-by-side on a 29 m horizontal boom, which is mounted on a 3 m diameter surface-piercing pile in water approximately 30(m) in depth. Assuming a 3:1 elliptical shape for the boom, the drag coefficient based on frontal area is approximately 0.17 in turbulent flow [12]. For a cylinder in turbulent flow, the drag coefficient based on frontal area is approximately 0.3 [12]. To use the above drag coefficients to determine the effect on efficiency, they are first renormalized with respect to the rotor swept area of 377(m^2) as shown in equations (12) and (13).

$$C_{D,boom} = \frac{L_{boom} w_{boom}}{A_R} 0.17 = \frac{29 \times 1}{377} 0.17 \qquad (12)$$

$$C_{D,pile} = \frac{L_{pile} w_{pile}}{A_R} 0.3 = \frac{30 \times 3}{377} 0.3 \qquad (13)$$

These drag coefficients are then used to calculate the effect of structural drag on the efficiency of the turbine, which is shown in Fig. 11 including the efficiency of the case 2 duct for comparison. It can be seen that structural drag may have a similar effect to the duct on the overall efficiency of the turbine.

VII. Conclusions

There is desire to improve the power coefficient of ducted turbines to achieve a greater power production with a smaller rotor spinning at faster rotational speeds to aid gearbox and generator operation. It is thought that this strategy will reduce the cost per kilowatt of tidal power generation. A trend in

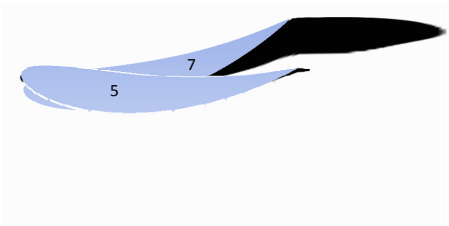

Figure 9: Separated flow regions behind ducts 5 and 7

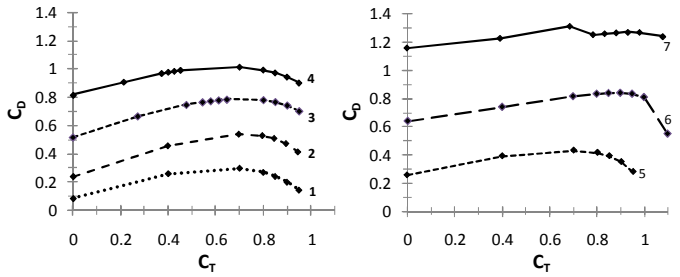

Figure 10: Drag coefficient for ducted designs

achieving this goal is to exploit the base pressure effect, which has been shown here to reduce the overall efficiency of the system.

For a small number of turbines installed in a large channel, there is no issue with exploiting the base pressure effect. In such a scenario, the level of power extraction would not be approaching any limit as described by Garrett. In fact, turbines using this approach may prove to be very economical since the turbine could be quite small compared to an open flow design giving the same average power. Setoguchi [13] has proposed duct designs which incorporate a brim at the duct trailing edge to intentionally create a large flow recirculation to induce the base pressure effect.

If tidal turbine farms are to be developed on a large scale however, the overall efficiency will become an important design parameter. One method of quantifying the environmental impact of tidal turbines is to model their effect on basin scale dynamics. Parameters of interest include the tidal range, total basin circulation and flow velocity. These parameters vary as the total power extracted from the flow increases. Placing restrictions on change in the tidal regime will impose limits to the total power extraction, which in turn necessitates a high overall efficiency. Therefore, for large scale generation, designs which use the base pressure effect are less suitable due to their inherently lower efficiency.

Observing the plots of efficiency and power coefficient, it can be seen that for each design there is an operating C_T which maximizes C_P, and a lower C_T which maximizes the efficiency. As the drag (be it structural or due to the duct) increases, the C_T for optimum efficiency tends to increase, but the peak efficiency is also reduced. This shows that any given turbine cannot operate at maximum power and maximum efficiency at the same time. For small scale generation, it is

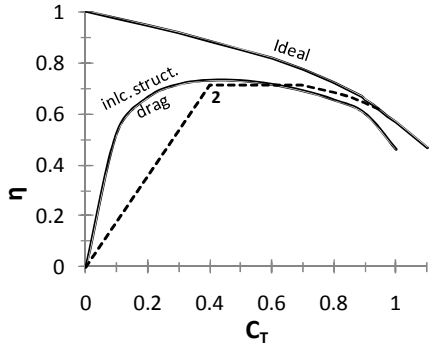

Figure 11: Effect of structural drag on efficiency

clear that it would be best to operate at maximum power. As the scale of power extraction approaches limits (either physical limits to the maximum possible extraction or limits to the acceptable change in tidal regime) it becomes more important to operate at the thrust coefficient for maximum efficiency.

Given the different requirements for designing small and large scale turbine arrays, it should be evident that as a tidal turbine farm grows, the type of turbines and the way they are operated should evolve towards more efficient machines. Based on the present results less aggressive duct designs seem more appropriate as efficiency becomes more critical.

The present study has neglected a number of important factors for determining the overall efficiency including: drag due to structural components, the effect of a discrete number of blades, blade tip loss, wake swirl, free surface effects and generator efficiency. Future work will involve quantifying the impact of these important phenomena on the overall turbine efficiency.

REFERENCES

[1] Sutherland G., Foreman M., Garrett C., *Tidal current energy assessment for Johnstone Strait, Vancouver Island*, Proc. IMechE Vol. 221 Part A: J. Power and Energy, 2007, pp. 147-157

[2] Karsten, R.H., McMillan J.M., Lickley M.J., Haynes R.D., *Assessment of tidal current energy in the Minas Passage*, Bay of Fundy, Proc. IMechE Vol. 222 Part A: J. Power and Energy, 2008, pp.493-507

[3] Polagye B., Kawase M., Malte P., *In-stream tidal energy potential of Puget Sound, Washington.* Proc. IMechE Vol. 223 Part A: J. Power and Energy, 2009, PP.571-587

[4] Garrett C., Cummins P., *Limits to tidal current power*, Renewable Energy, Vol. 33, 2008, pp. 2485–2490

[5] Burton, T., Sharpe, D., Jenkins, N. and Bossanyi., E., *Wind Energy Handbook :* John Wiley & Sons Ltd., 2001.

[6] Corten, G.P., *Heat Generation by a Wind Turbine.* 14th IEA symposium on the aerodynamics of wind turbines, 2000

[7] Hansen M.O.L., Sorensen N.N., Flay R.G.J., *Effect of Placing a Diffuser around a Wind Turbine*, Wind Energy, Vol. 3, 2000, pp.207-313

[8] van Bussel, G.J.W., *The science of making more torque from wind: Diffuser experiments and theory revisited*. Journal of Physics: Conference Series, 2007, Vol. 75. pp. 1-12

[9] Lawn, C.J., *Optimization of the power output from ducted turbine*. Proc. Instn. Mech. Engrs. Vol. 217 Part A: J. Power and Energy, 2003, pp. 107-117.

[10] Jamieson, P., *Generalized Limits for Energy Extraction in a Linear Constant Velocity Flow Field.* Wind Energy, Vol. 11, 2008, pp. 445-457.

[11] Sea Generation Ltd, *SeaGen Fact Sheet*, Marine Current Turbines, Online: http://www.seageneration.co.uk/downloads.asp Accessed: June 2010.

[12] White, F.M., *Fluid Mechanics*. 5th ed., McGraw Hill, 2003. ISBN: 0-07-240217-2.

[13] Setoguchi, T., Shiomi, N., and Kaneko, K., *Development of two-way diffuser for fluid energy conversion system.* Renewable Energy, 2004, Vol. 29. pp. 1757-1771